Supplementary Material (ESI) for Green Chemistry

Supporting Information for

Base-Free aerobic oxidation of 5-hydroxymethylfurfural to 2, 5-furandicarboxylic acid over a Fe single-atom catalyst

Sohaib Hameed [a,b], Wengang Liu [c*], Zhounan Yu [a], Jifeng Pang [a], Wenhao Luo [a,d*] and Aiqin Wang [a*]

[a] *CAS Key Laboratory of Catalysts and New Materials, Dalian Institute of Chemical Physics, Chinese Academy of Sciences, 457 Zhongshan Road, Dalian 116023, P.R. China*

[b] *University of Chinese Academy of Sciences, Beijing 100049, P.R. China*

[c] *College of Material Science and Engineering Qingdao, University of Science and Technology, Qingdao 266042, P.R. China*

[d] *College of Chemistry and Chemical Engineering, Inner Mongolia University (Inner Mongolia), Hohhot 010021, P. R. China.*

[*] *Corresponding authors. E-mail addresses: aqwang@dicp.ac.cn; w.luo@imu.edu.cn; liuwengang@qust.edu.cn*

Materials

All the reagents in this study were commercialized and used as received without any further treatment. Iron Acetate ($Fe(OAc)_2$, Purity: >90%), alumina (Al_2O_3, type: γ, Size: 20 nm, Purity: 99.99% on metal basis), magnesium oxide (MgO, Size: 50nm, Purity: 99.9% on metal basis) and zirconium dioxide (ZrO_2: Size: ≤ 100nm, Purity; 99.99% on metal basis) were purchased from Shanghai Aladdin Biochemical Technology, Shanghai, China. Titanium oxide (TiO_2, Type: P-25, Purity: 99.9%) was purchased from Tianjin baima technology, Tianjin, China. 1,10 phenanthroline (Purity: ≥99%) from Tianjin Kemiou Chemical Reagent Company Limited, Tianjin, China. Aforementioned all chemicals were used for preparation of catalysts. Chemical reagents applied for catalytic reaction are; 5-hydroxymethylfurfural (HMF, Purity: >99%) was purchased from Shanghai Aladdin Biochemical Technology, Shanghai, China. Dimethyl sulfoxide (DMSO Purity: 99.5%) from Damao chemical Reagent, oxygen gas (O_2, Purity: 99.9%) was purchased from Dalian Kerui Gas Co., Ltd. Commercialized oxidation products for this reaction were also purchased for standard curves. 2,5-diformyl-furan (DFF, Purity: 98%) was purchased from Shanghai Macklin Biochemical company Limited , 5-hydroxymethyl-2-furan carboxylic acid (HMFCA, Purity: 98.93%) from Ark Pharm, 5-formyl-2-furan carboxylic acid (FFCA, Purity: 98%) from bide pharm and 2,5-furandicarboxylic acid (FDCA, Purity: 98%) from Shanghai Aladdin Biochemical Technology, Shanghai, China.

Characterization of catalysts

X-ray diffraction (XRD)

Crystalline phases of catalysts were identified by XRD analysis which was performed on a PANalytical X'pert PRO x-ray diffractometer equipped with a Cu Kα radiation source (λ = 1.58418Å) and a nickel filter. Beam voltage was operated at 40kV and 40mA and diffractograms were recorded with scanning angle (2θ) domain of 10^o to 90^o along with measured rate of 0.02^o per second sampling interval. PANalytical X'pert High Score and JADE software were used for analyzing the data. JCPDS database was used to interpret the diffractograms.

Inductively Coupled Plasma Mass Spectroscopy (ICP-MS)

The actual metal loadings of the prepared catalysts and metal leaching after catalytic reactions were determined using ICP-MS technique. This spectroscopy was performed on IRIS Interpid (II) XSP instrument of Thermo electron corporation. A sufficient quantity of the powder catalyst sample was treated in hot aqua regia (HCl: HNO_3; 3:1) to dilute the sample before ICP-MS analysis.

Scanning transmission electron microscopy (STEM)

STEM and High angle annular dark-field (HAADF) STEM images were obtained on a JEOL JEM-ARM200F microscope operated at an acceleration voltage of 200 kV with a guaranteed resolution of 0.08 nm. Before this characterization, the catalysts samples were suspended in ethanol and dispersed ultrasonically. Then drops of prepared suspension were applied onto the copper grids covered with lacy carbon films and finally dried at room temperature. Elemental mapping and energy dispersive spectroscopy (EDS) layered images were obtained on X-MAXN 80 T IE-250 instrument.

N_2 adsoption-desorption

The textural properties of the calcined catalyst samples were identified from N_2 adsoption-desoption isotherms which were obtained at -196 ^oC using a Micromeritics ASAP 2460 instrument. To determine the pore size distribution, the Barrett-Joyner-Halenda (BJH) method was used while the t-plot approach was used to compute the pore volumes. Prior to the measurements, the samples were degassed overnight with N_2 flow at 200 ^oC and 1 mTorr to ensure a relatively clean surface. Brunauer-Emmett-Teller (BET) surface areas were calculated from adsorption isotherm data within the equilibrium pressure range of $0.05<P/P_o<0.3$.

Temperature Programmed Desorption

NH_3-TPD

The measurements regarding acidic sites distribution and surface acidity of catalysts were analyzed by temperature programed desorption of NH_3 (NH_3-TPD). Micrometrics Autochem II 2920 instrument was used coupled with MS detector. To perform the NH_3 TPD experiments, firstly catalyst samples were put in a quartz reactor of TPD instrument and pretreated under 30 mL/min flow of He gas at 400 ^oC for 2 h, then allowed it to cool down at 50 ^oC. Secondly, the NH_3 adsorption step was carried out at 50 ^oC by feeding 10%

NH_3/He (30 mL/min) flow until saturation. Then the sample chamber was flushed out with He for 60 min to remove the weakly adsorbed NH_3 from the catalytic surface. After the base line of MS signal became steady, the NH_3 desorption was performed from 50 to 850 ^oC with heating temperature ramp of 10 ^oC/min and finally desorbed NH_3 was monitored at MS detector. Effluent curves of desorbed NH_3 were recorded and are known as NH_3-TPD curves.

CO_2-TPD

The measurements regarding basic sites distribution and surface basicity of catalysts were analyzed by temperature programed desorption of CO_2 (CO_2-TPD). Micrometrics Autochem II 2920 instrument was used coupled with thermal conductivity detector (TCD). To perform the CO_2 TPD experiments, firstly catalyst samples were put in a quartz reactor of TPD instrument and pretreated under 30 mL/min flow of He gas at 400 ^oC for 2 h, then allowed it to cool down at 50 ^oC. Secondly, the CO_2 adsorption step was carried out at 50 ^oC by feeding 100%CO_2 (50 mL/min) flow until saturation. Then the sample chamber was flushed out with He for 60 min to remove the weakly adsorbed CO_2 from the catalytic surface. After the base line of TCD signal became steady, the CO_2 desorption was performed from 50 to 850^oC with heating temperature ramp of 10 ^oC/min and finally desorbed CO_2 was monitored at TCD detector. Effluent curves of desorbed CO_2 were recorded and are known as CO_2-TPD curves.

X-ray absorption spectroscopy (XAS)

X-ray absorption spectroscopy (XAS) of the Fe-K edge was measured using the XAFS instrument BL 14W1 of Shanghai Synchrotron Radiation Facility (SSRF) at Shanghai institute of applied physics (SINAP) Shanghai, China. The energy of electron beam was 3.0 GeV with a ring current of ~300 mA. The data for all three main regions of XAS spectra including X-ray absorption near-edge structure (XANES) region and extended X-ray absorption fine structure (EXAFS) region, was collected on transmission mode at room temperature. The incident X-ray was monochromatized by a Si (111) double-crystal monochromator and detuned by 30 % to reduce undesired harmonics. Fe foil was measured concurrently as reference to calibrate each sample. All XAS data were analyzed using ATHENA and AREMIS software packages.

Mössbauer Spectroscopy

^{57}Fe Mössbauer spectra of the catalysts were carried out on a Topologic 500A spectrometer driving with a proportional counter at room temperature. The radioactive source was ^{57}Co (Rh) moving in a constant acceleration mode. Data analyses were performed assuming a Lorentzian line shape for computer folding and fitting. The components of iron phases were identified based on their Mössbauer parameters including isomer shift (δ), quadruple splitting (ΔE_Q) and magnetic hyperfine field.

Xray-photoelectron spectroscopy (XPS)

X-ray photoelectron spectroscopy (XPS) measurements for all four catalysts was carried out on a Thermo Scientific ESCALAB 250Xi spectrometer equipped with an Al anode (Al Kα = 1846.6 eV). The background pressure in the analysis chamber was lower than 1×10^{-8} Pa, and the operating pressure was around 1.5×10^{-5} Pa. The survey and spectra were acquired at a pass-energy of 30 eV. The binding energy (B.E.) calibration was adjusted bases on a reference peak of C 1s transition appeared at 284.6 eV.

Diffuse reflectance infrared Fourier transform (DRIFT) spectra

Diffuse reflectance infrared Fourier transform (DRIFT) spectra were collected with a Vertex 70 V spectrometer (Bruker Optics) equipped with a liquid-nitrogen cooled mercury cadmium telluride (MCT) detector with a resolution of 4 cm^{-1} and a commercial mirror unit (PIKE Technologies, DiffusIR). All spectra were recorded at 20 °C unless otherwise noted. Before the collection, the samples were treated with ultrapure He at 200 °C for 30 min to remove water and then cooled to room temperature to record the background spectra. The quartz cell was used at room temperature to bubble HMF solution throughout the measurements. 0.08M HMF solution was flown over the catalyst layer by pure He at a rate of 0.6 mL/min using a peristaltic pump located next to the quartz cell. The powder samples of catalysts were used without further dilution. Spectra were ratioed against a background spectrum recorded in He flow prior to admittance of HMF bubbles. Infrared spectra were collected in the 4000-1000 cm^{-1} spectral range every 30 s (30 scans) at 4 cm^{-1} resolution. All infrared spectra (DRIFT) are presented in the form of the Kubelka-Munk function.

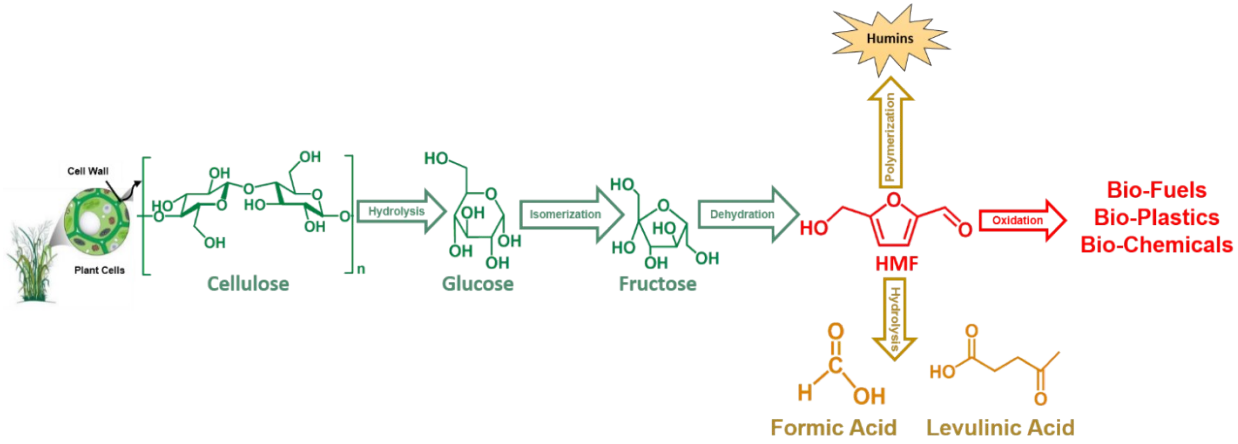

Figure S1. Schematic illustration of HMF synthesis from cellulose via isomerization of glucose and dehydration of Fructose

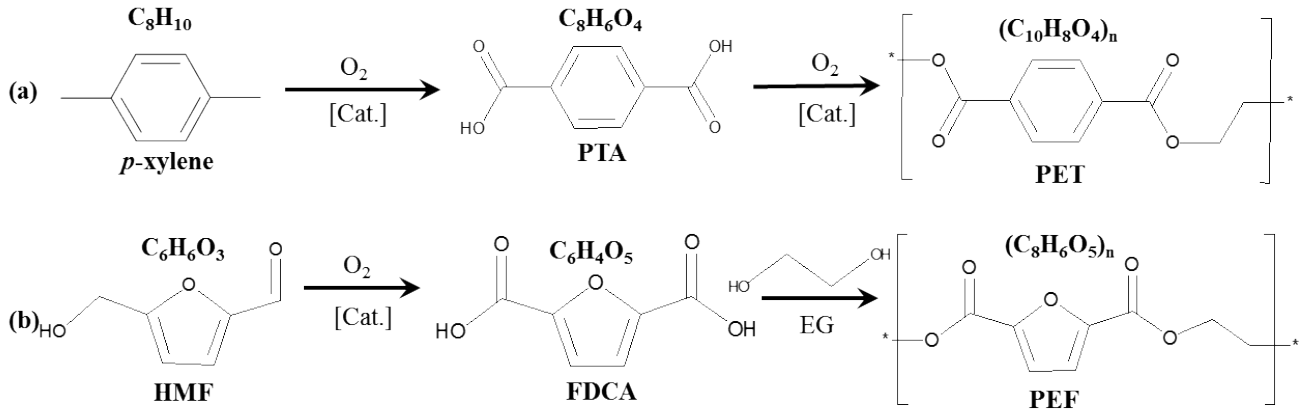

Figure S2. Structural comparison for production of petroleum-derived PET and biomass-derived PEF.

Table S1. Summary of reported studies on Fe-based catalysts for catalytic oxidation of HMF to FDCA

Catalysts	Additive	Reaction Conditions			HMF Conv. (%)	FDCA Yield (%)	Ref.
		T (°C)	Oxidant P (bar)	Time (h)			
NiFeS	CH_3CN	120	t-BuOOH	12	100	83.2	1

NiFeP-400	CH_3CN	120	t-BuOOH	12	100	82.7	1
FeNPs@NH_2-SBA-15	Base Free	120	O_2, 06	14	100	89.4	2
10Fe@22NB@MNP	Base Free	100	t-BuOOH	12	99.7	94.1	3
$Fe_{0.6}Zr_{0.4}O_2$	[Bmim]Cl	160	O_2, 20	24	99.7	60.6	4
$Ce_{0.5}Fe_{0.5}O_2$	[Bmim]Cl	140	O_2, 20	24	98.4	13.8	5
$Ce_{0.5}Zr_{0.5}O_2$	[Bmim]Cl	140	O_2, 20	24	96.1	23.2	5
$Ce_{0.5}Fe_{0.15}Zr_{0.35}O_2$	[Bmim]Cl	140	O_2, 20	24	99.9	44.2	5
Fe_3O_4-CoO_x	Base Free	80	t-BuOOH	12	97.2	68.6	6
Fe^{III}-POP-1[a]	Base Free	100	O_2, 10	10	100	79.0	7

[a] POP = Porous organic polymer

[b] MR-Co-Py = Merrifield Resin supported Co(II)-meso-tetra(4-pyridyl-porhyrin)

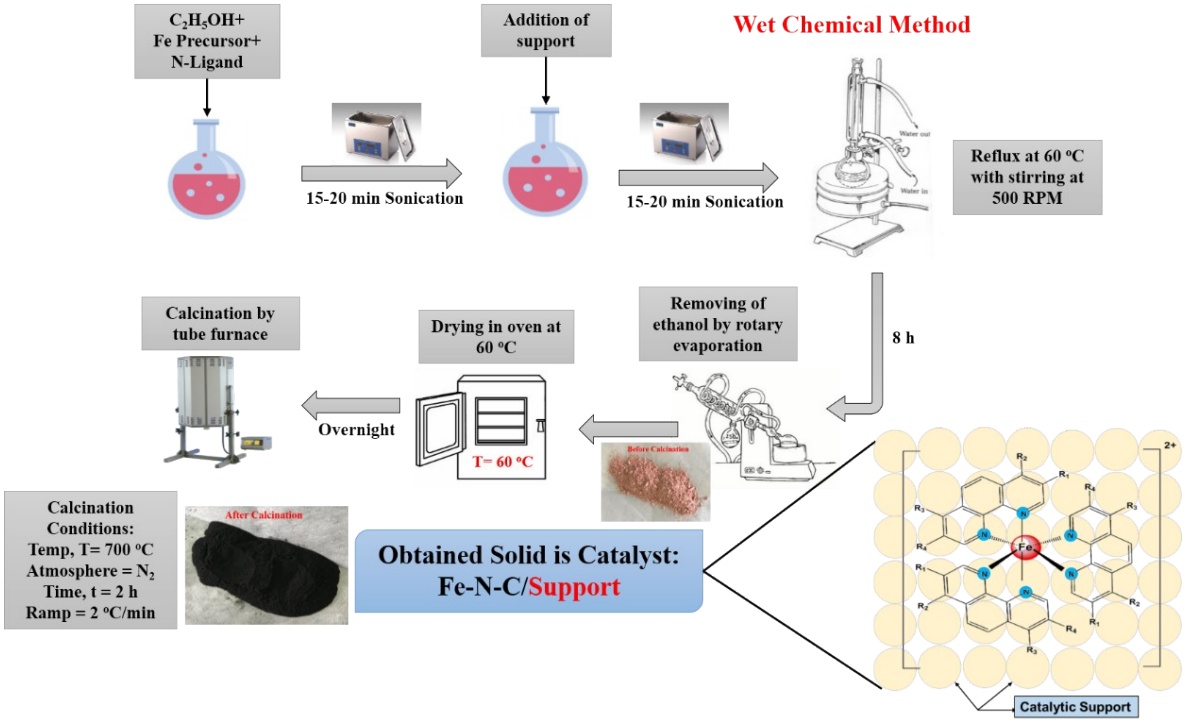

Figure S3. Steps for preparation of catalysts

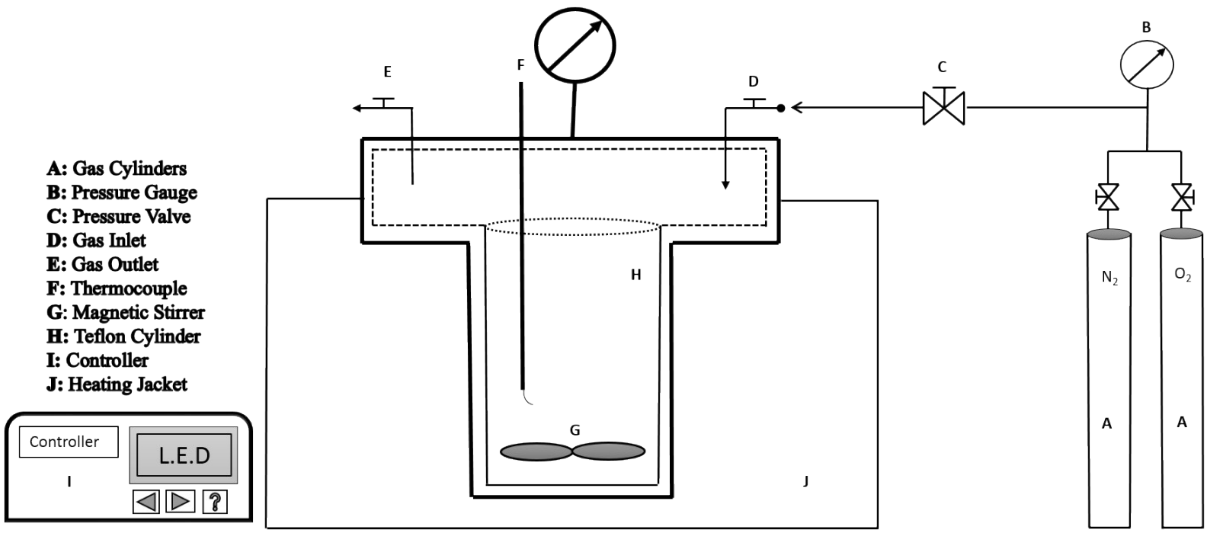

Figure S4. Schematic illustration of reaction system

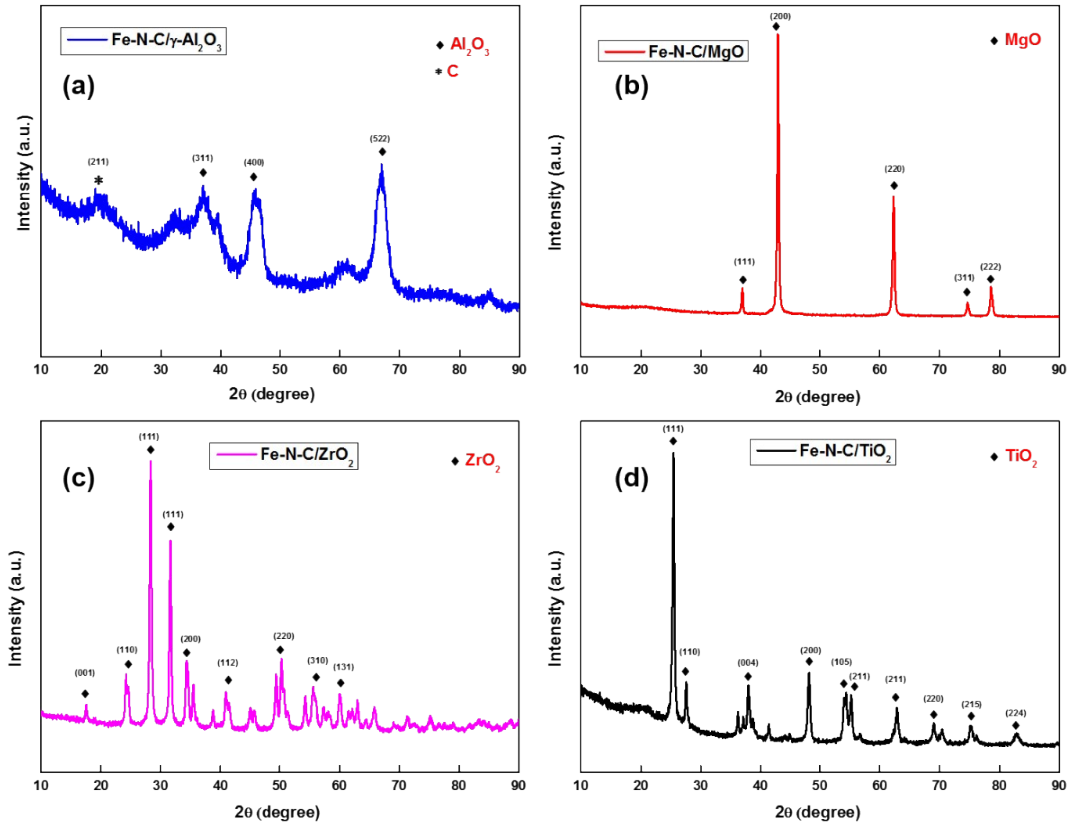

Figure S5. XRD patterns of Fe-N-C catalysts over four different supports. All four samples are calcined at 700 ^{o}C for 2 h in N_2 atmosphere.

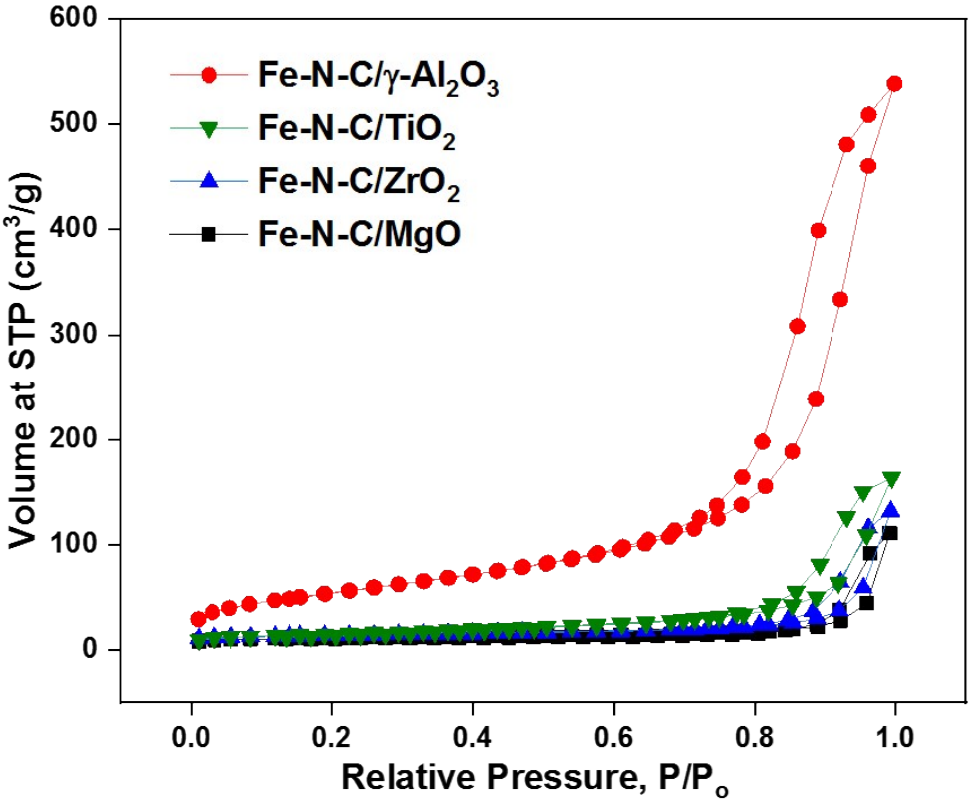

Figure S6. N_2-Physisorption Isotherms for the three catalysts describing surface areas using BET method

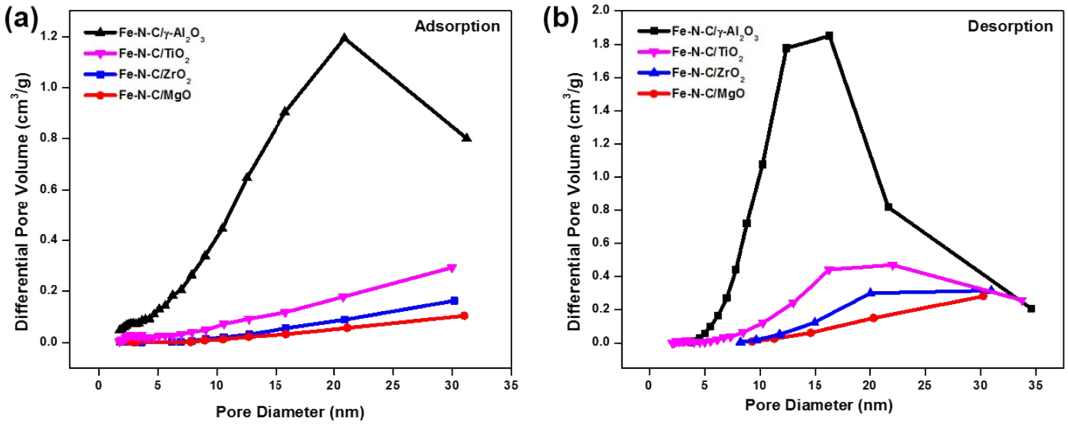

Figure S7. BJH Pore size distribution plot for Fe-N-C catalysts derived from **(a)** adsorption and **(b)** desorption of N_2-sorption isotherms.

Table S2. N_2-Physisorption and ICP-MS results of supported Fe-N-C catalysts calcined at 700 °C for 2 h in N_2 atmosphere.

Catalysts	Fe Loading (Theoretical) (wt %)	Fe Loading (Experimental) (ICP-MS) (wt %)	Surface Area (BET) (m^2/g)	Pore Volume (BJH) cm^3/g	Avg. Pore Diameter (BJH) (nm)
Fe-N-C/γ-Al_2O_3	1	0.92	197.8	0.79	13.6
Fe-N-C/TiO_2	1	0.97	53.3	0.25	17.9
Fe-N-C/ZrO_2	1	0.93	44.6	0.19	25.4
Fe-N-C/MgO	1	0.94	37.1	0.16	28.6

**Pore Volume and Pore diameter was measured using Desorption Isotherms*.

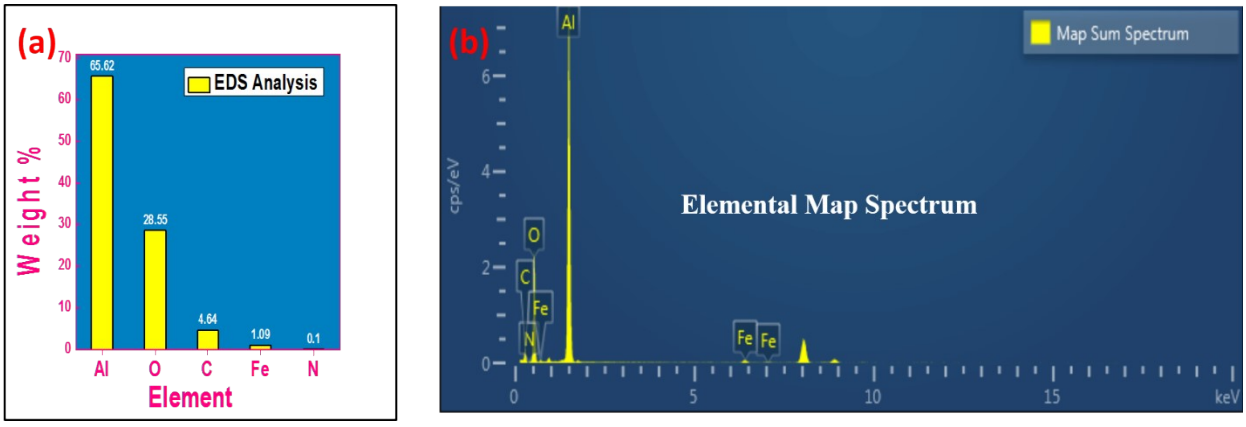

Figure S8. (a) Elemental composition using EDS analysis **(b)** Elemental map spectrum of Fe-N-C/γ-Al_2O_3 catalyst

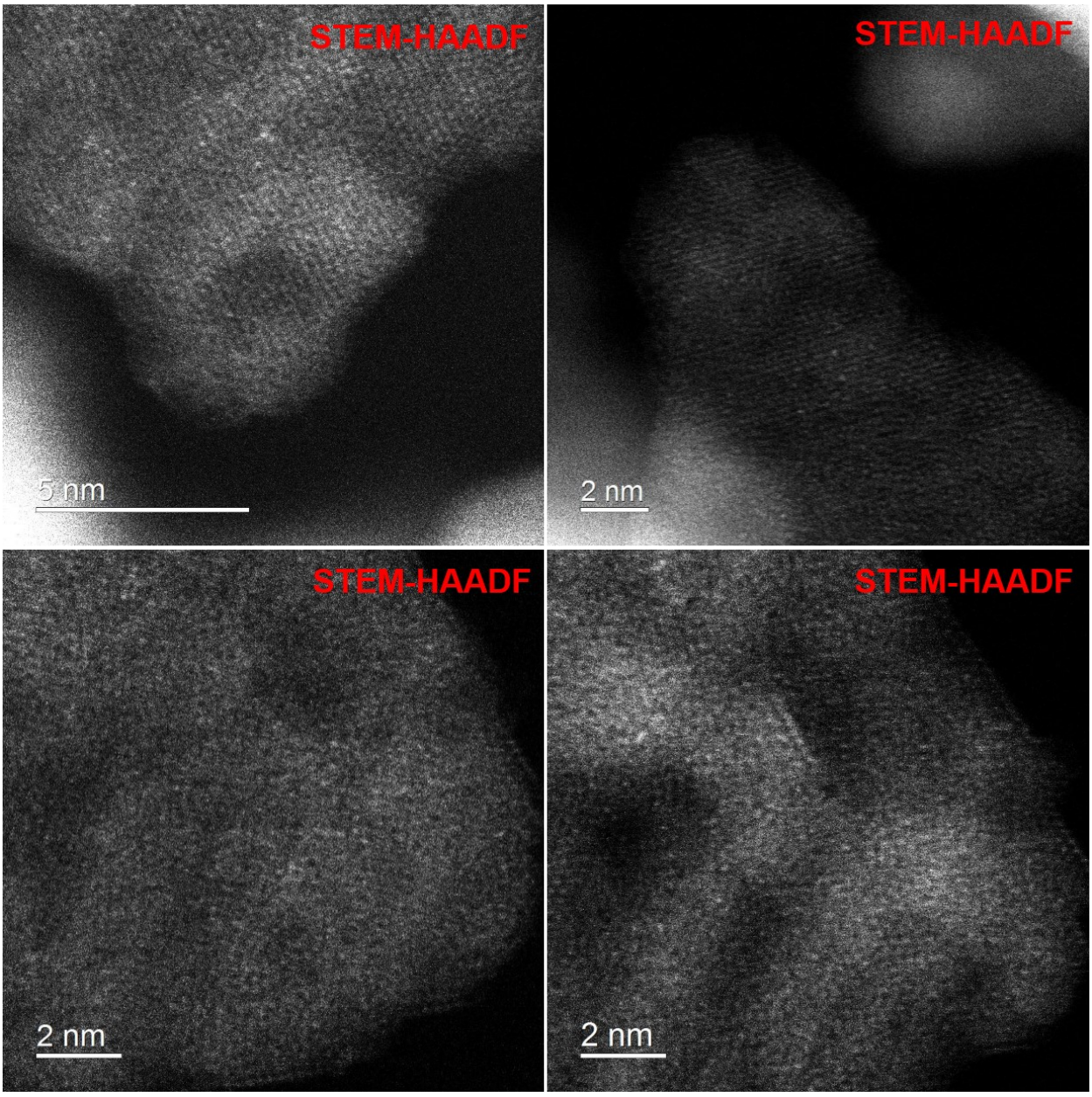

Figure S9. HAADF-STEM images of Fe-N-C/γ-Al_2O_3 catalyst

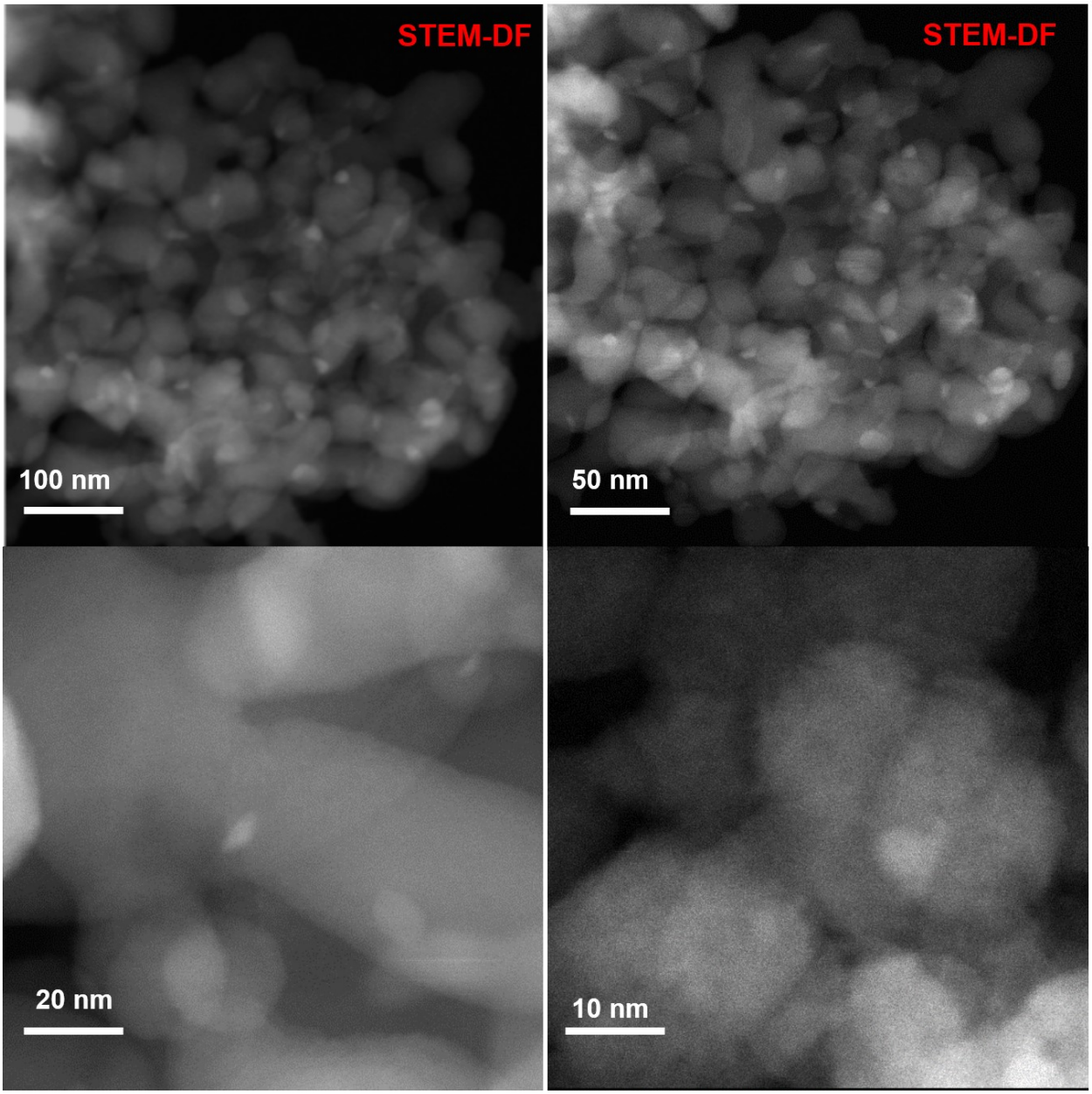

Figure S10. STEM-DF images of Fe-N-C/MgO catalyst

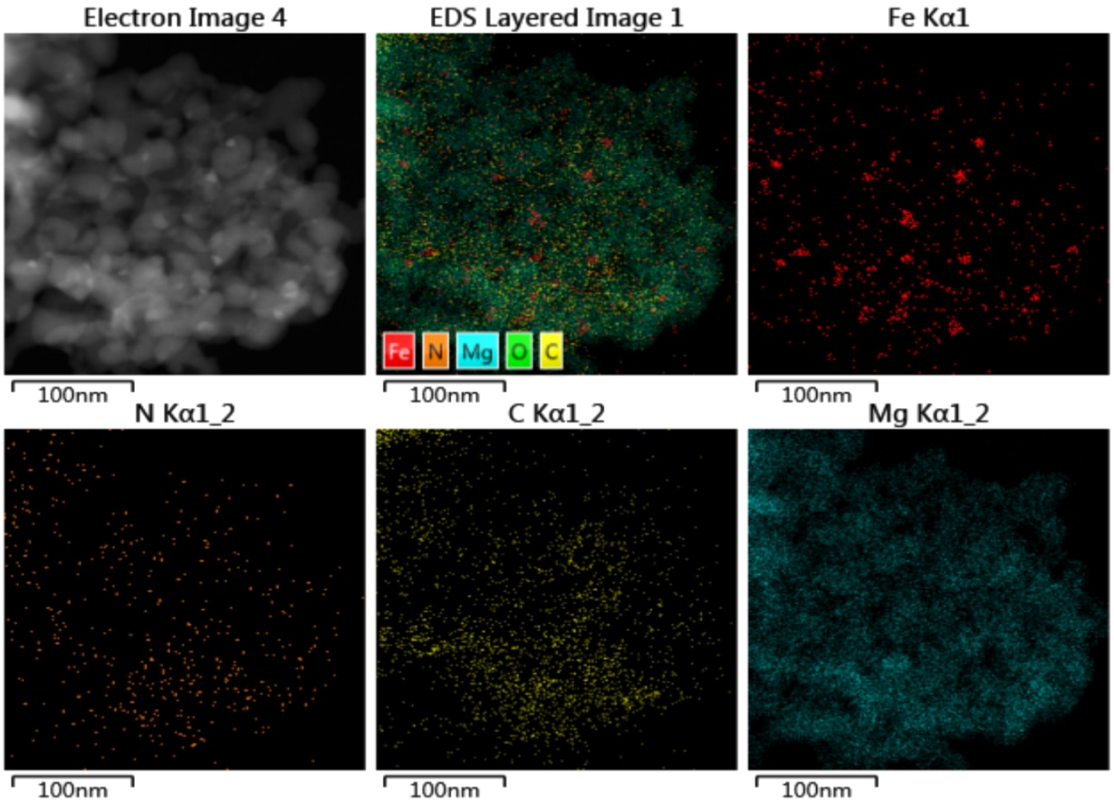

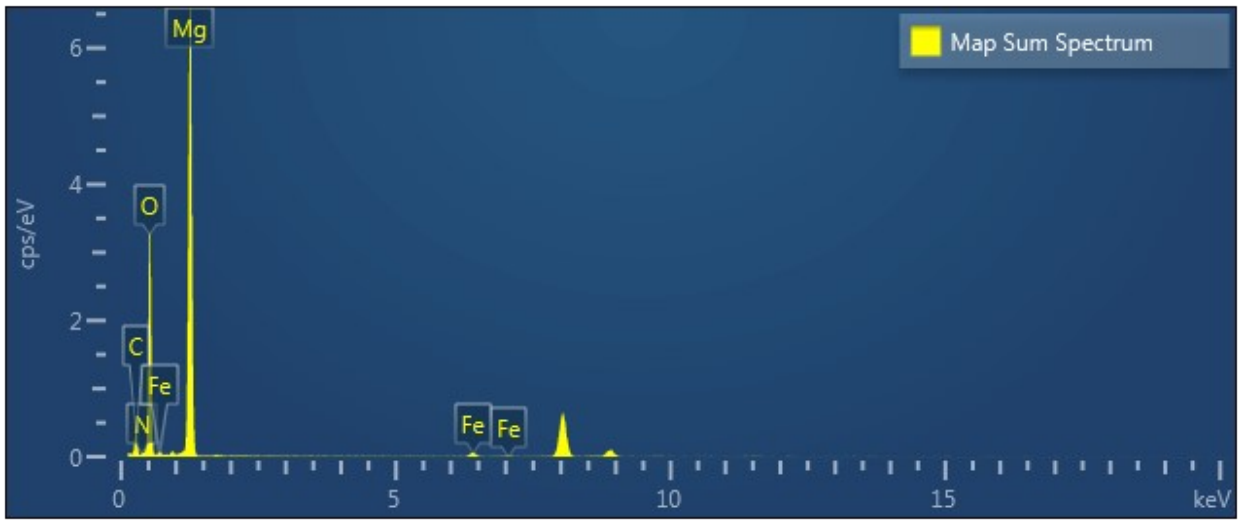

Element	Line Type	k factor	Absorption Correction	Wt%	Wt% Sigma
C	K series	2.50675	1.00	5.76	0.21
N	K series	3.14061	1.00	0.43	0.18
O	K series	1.86867	1.00	38.62	0.30
Mg	K series	1.06408	1.00	54.12	0.31
Fe	K series	1.19079	1.00	1.07	0.06

Total:				100.00	

Figure S10A. Elemental mapping, map sum spectrum and elemental composition of Fe-N-C/MgO catalyst using EDS-analysis.

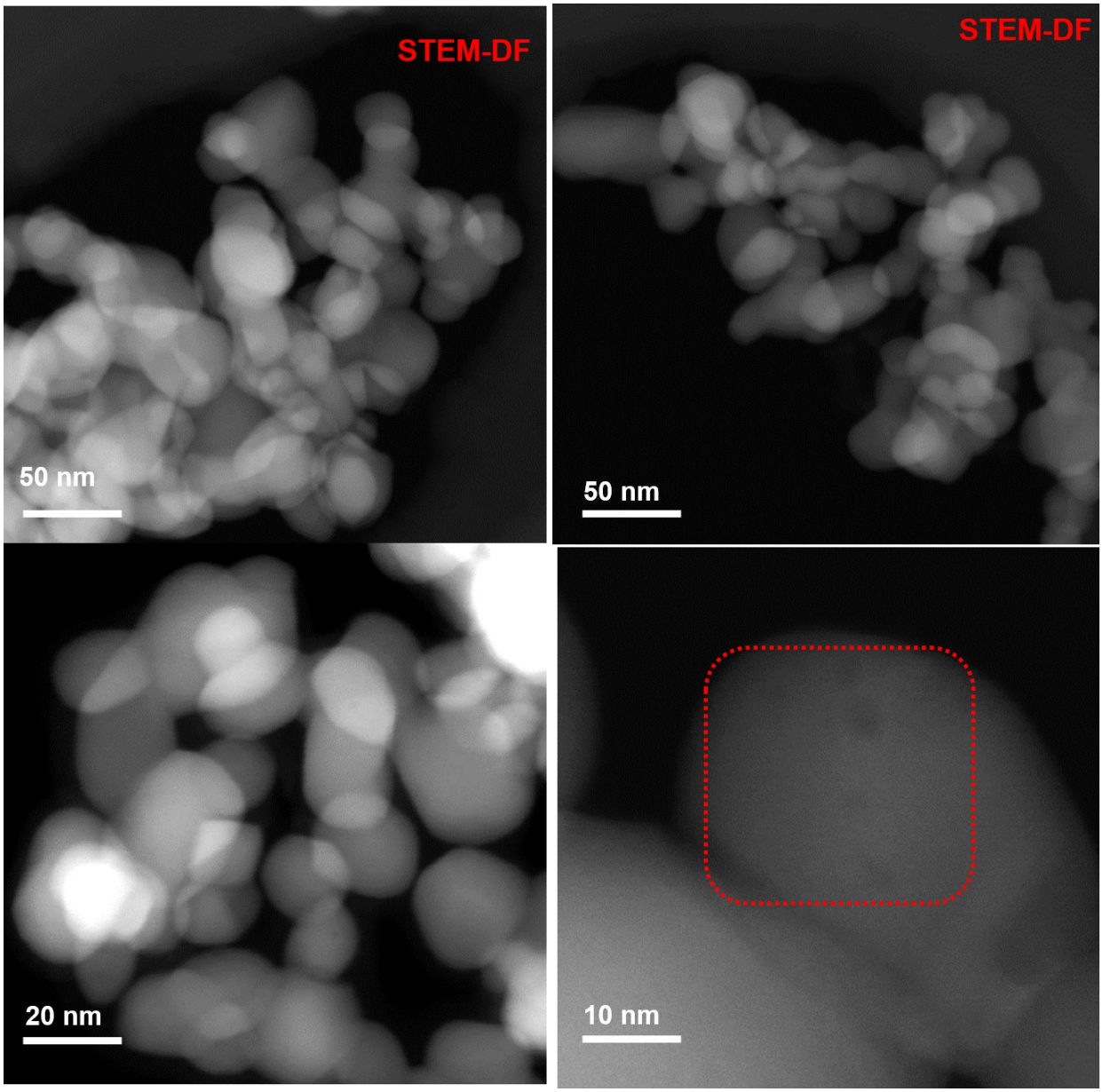

Figure S11. STEM-DF images of Fe-N-C/ZrO_2 catalyst

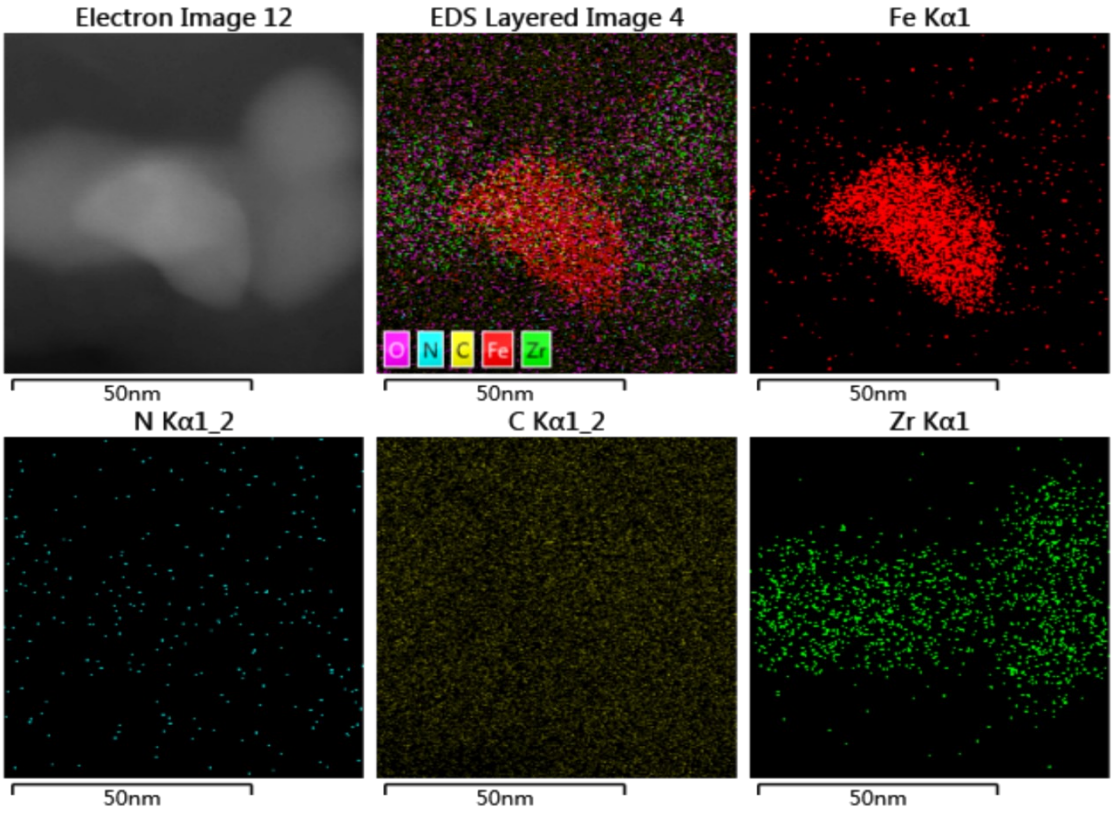

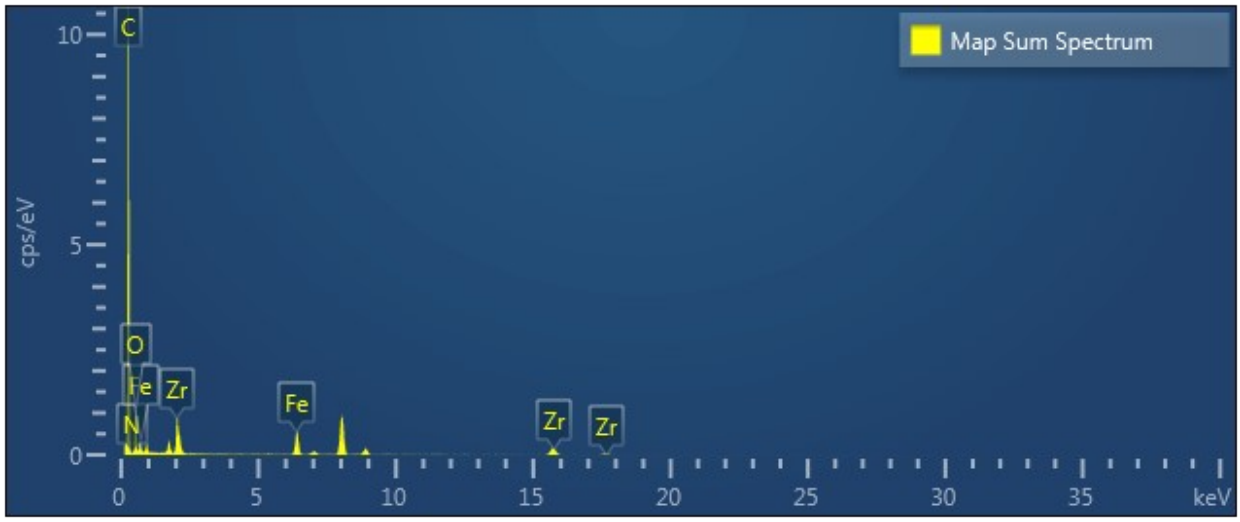

Element	Line Type	k factor	Absorption Correction	Wt%	Wt% Sigma
C	K series	2.50675	1.00	79.18	0.35
N	K series	3.14061	1.00	0.00	0.00
O	K series	1.86867	1.00	6.25	0.17

Fe	K series	1.19079	1.00	4.68	0.12
Zr	L series	1.73589	1.00	9.89	0.33
Total:				100.00	

Figure S11A. Elemental mapping, map sum spectrum and elemental composition of Fe-N-C/ZrO_2 catalyst using EDS-analysis.

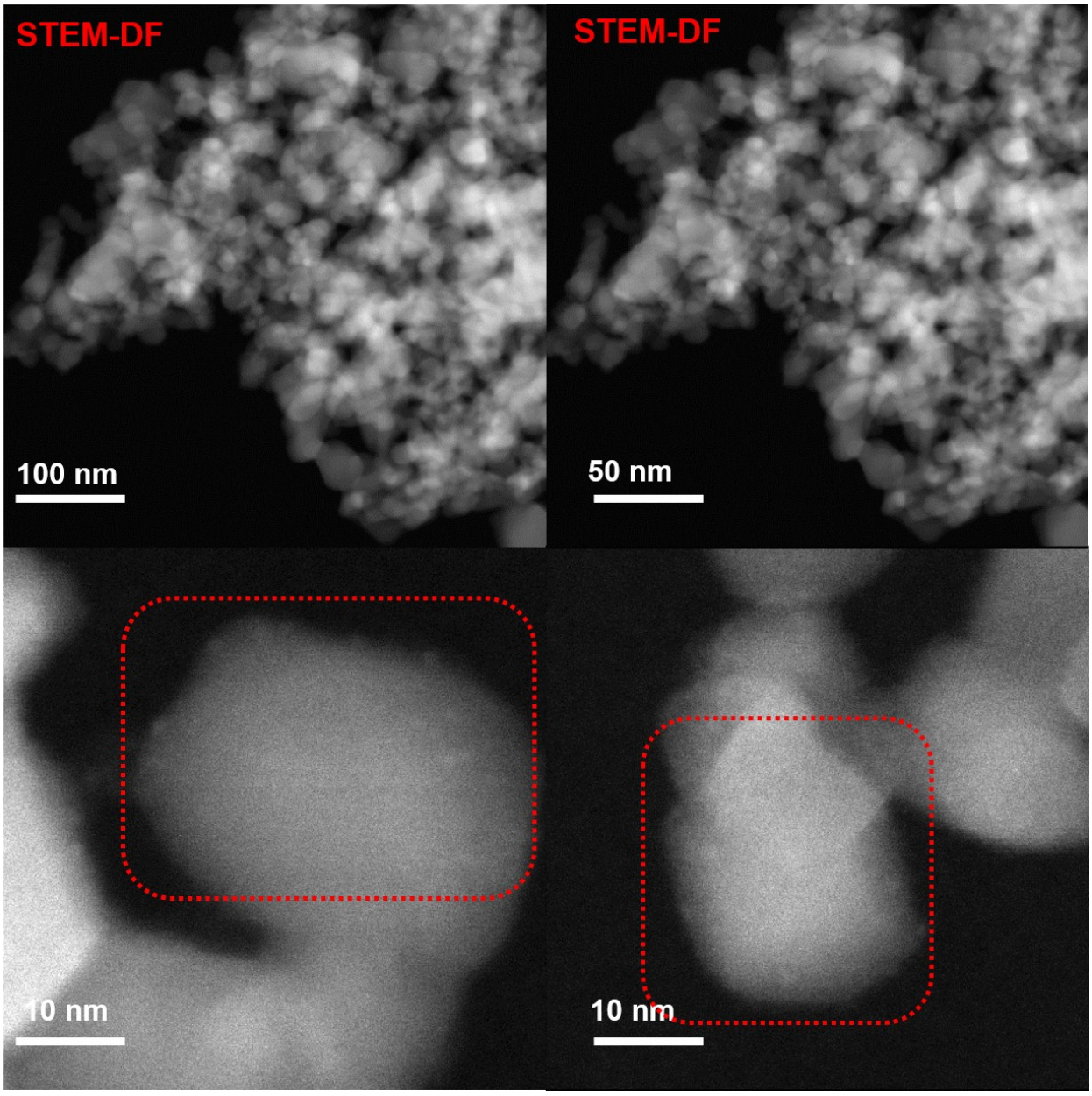

Figure S12. STEM-DF images of Fe-N-C/TiO_2 catalyst.

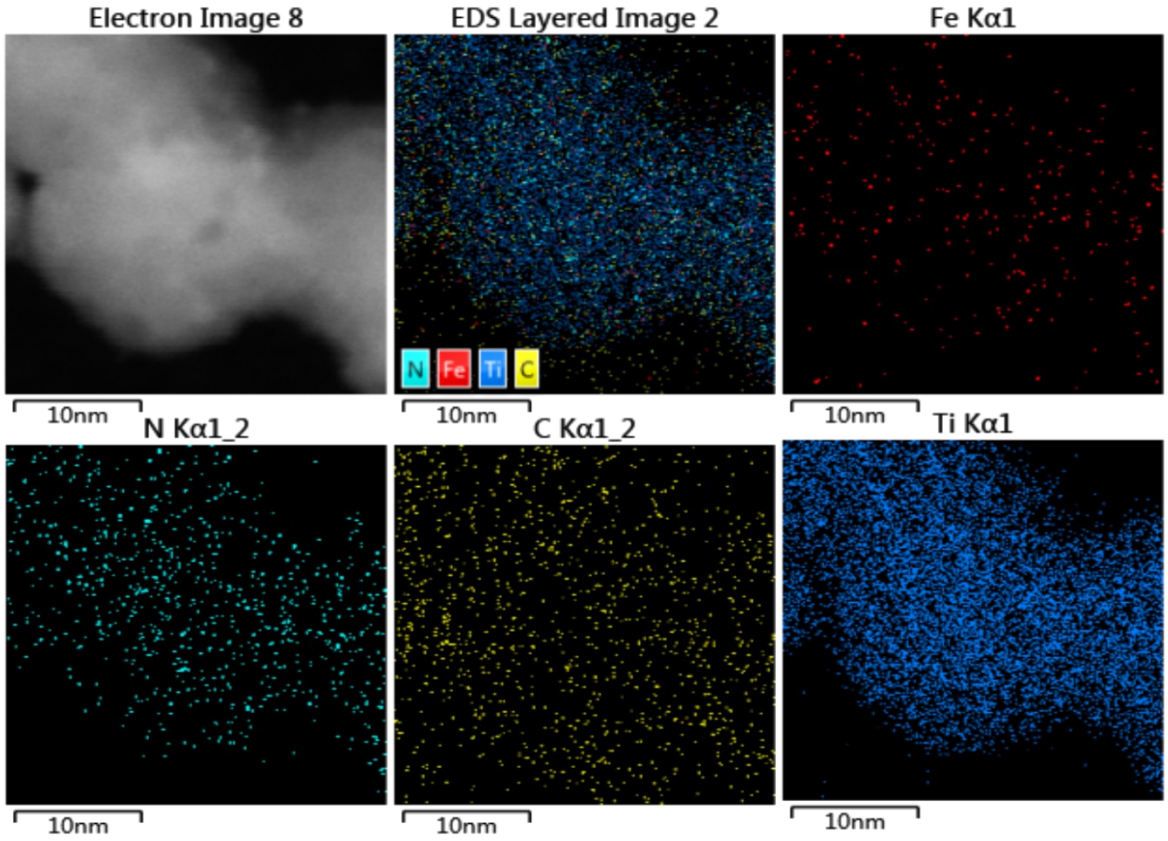

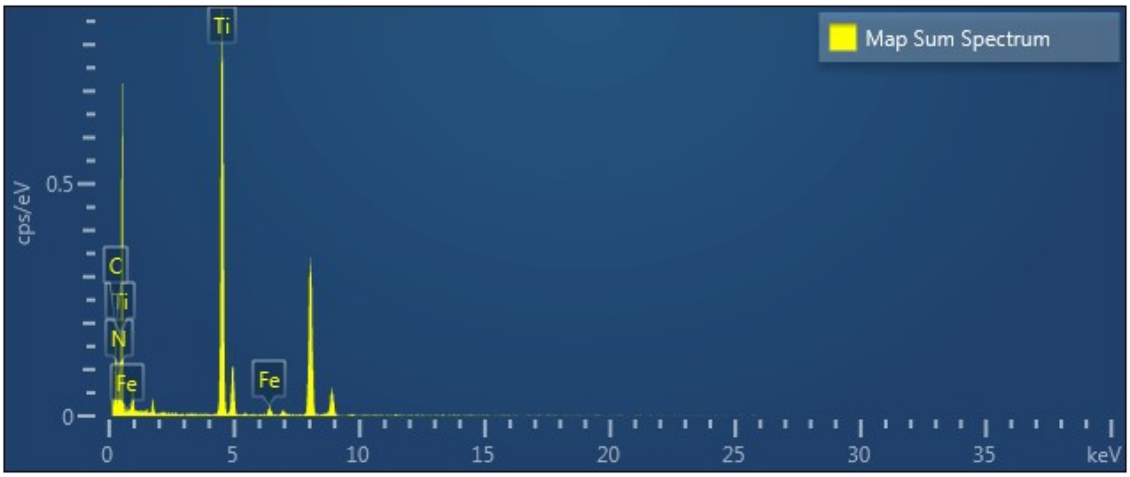

Element	Line Type	k factor	Absorption Correction	Wt%	Wt% Sigma
C	K series	2.50675	1.00	17.38	0.77
N	K series	3.14061	1.00	17.93	1.36

Ti	K series	1.06845	1.00	63.21	1.21
Fe	K series	1.19079	1.00	1.48	0.20
Total:				100.00	

Figure S12A. Elemental mapping, map sum spectrum and elemental composition of Fe-N-C/TiO_2 catalyst using EDS-analysis.

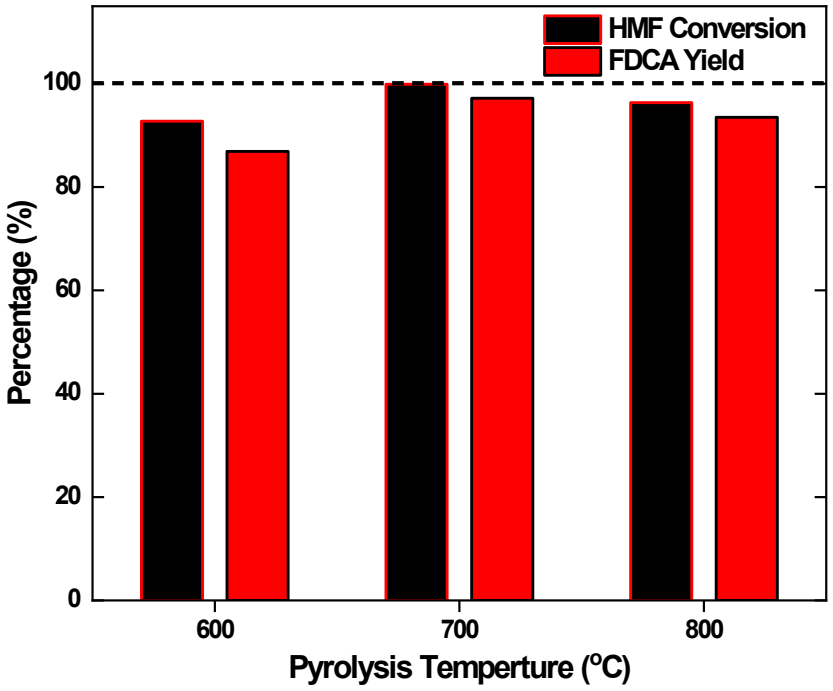

Figure S13. Effect of pyrolysis temperature of the gamma-alumina supported Fe-N-C catalyst after 15 h of reaction time. Reaction conditions: HMF = 0.8 mmol, Catalyst = 150 mg, HMF/Fe 30:1, 10 g DMSO/H_2O, T = 110 °C, P = 40 bar O_2, 700RPM

The catalytic properties of supported catalysts could significantly affect by the pyrolysis temperature.[8] In this study, a highly active Fe-N-C/γ-Al_2O_3 catalyst was subjected to pyrolysis at various temperatures (600 °C, 700 °C and 800 °C) in N_2 atmosphere with gas flow of 2 mL/min for two hours. The resulting catalytic performances were measured for selective oxidation of HMF to FDCA at 110 °C after 15 hours of reaction. As shown in Figure S7, more than 90% of HMF conversion was achieved for all the catalysts. More specifically, when the catalyst was calcined at 700 °C, greater than 99% of HMF was converted to products. However, at lower (600 °C) and higher (800 °C) temperatures, the HMF conversion achieved is 92.8% and 96.3%, respectively.

Moreover, the yield of desired product FDCA had similar behaviour as the yield obtained from the calcined sample at 700 °C was superior (97.2%) as compared to other two catalysts (86.9% and 93.5%). This variation in catalytic activity with calcination temperature may be due to the structural characteristics of Fe-N-C/γ-Al_2O_3 catalyst, such as crystallinity, BET surface area and the lattice oxygen mobility which are discussed in the later sections. These results demonstrated that the catalyst Fe-N-C/γ-Al_2O_3, calcined at 700 °C, exhibited the best performance for oxidizing HMF to FDCA. In order to conduct a further comparative investigation, Fe-N-C/γ-Al_2O_3 (Pyrolysis = 700 °C, N_2, 2h) was chosen.

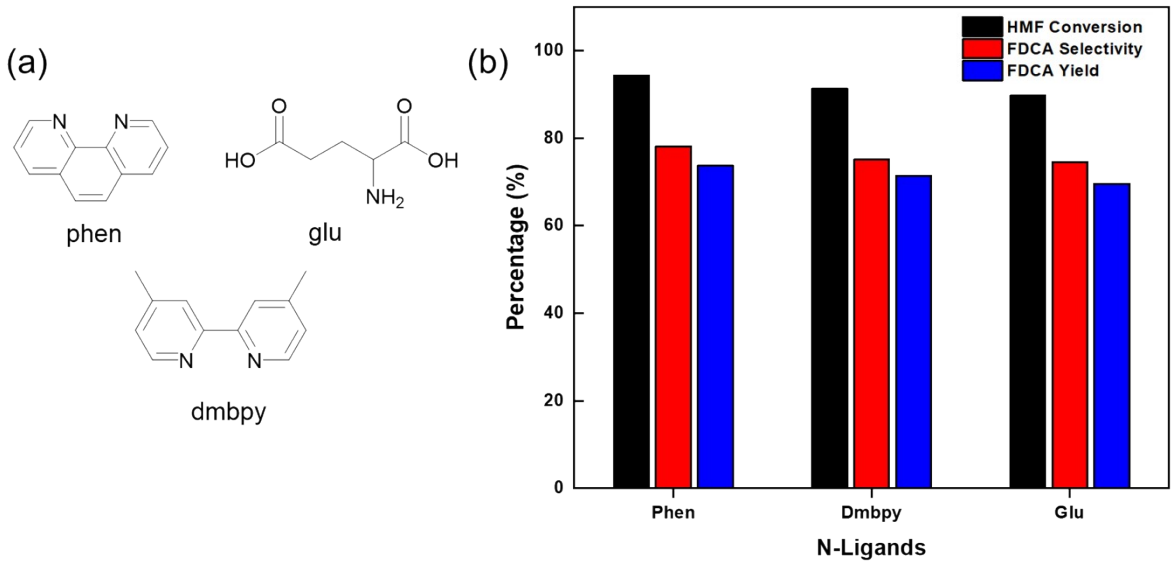

Figure S14. (a) Structures of N-ligands used to optimize the N-donor for optimal catalyst **(b)** Catalytic performance as a function of various N-ligands after 8 h of reaction at T = 110 °C and P(O_2) = 40 Bar.

Different N-containing ligands were tested during the catalyst preparation together with iron acetate salt to prepare Fe-N-C/γ-Al_2O_3 catalyst and perform an 8-hour reaction for HMF oxidation to form FDCA. 1,10-Phenanthroline (phen), 4,4'-Dimethyl-2,2'-bipyridine (dmbpy) and glutamic acid (glu) were tested and results are summarized in Figure S8. The conversions of HMF and FDCA yields for all N-donors showed essentially comparable results, indicating that the iron complexes produced from these ligands are very active and are more likely attributable to the higher association constants. The reason behind this is certainly the electron-withdrawing and donating effects of the substituents on the pyridine ring. As can be seen in the Figure S14, enhanced HMF conversion (78.2%) and FDCA yield (73.7%) was found if phen was used as N-ligand as

compared to its counter parts dmbpy and Glu which depicted 75.2% and 74.6% of HMF conversions and 71.4% and 69.6% of FDCA yields respectively. Phen can be utilized as a N-donor to create iron complexes in the catalyst, which was also found to slightly improve FDCA yield. As a result of these findings, all optimal catalysts were prepared using 1,10-Phenanthroline as the N-ligand.

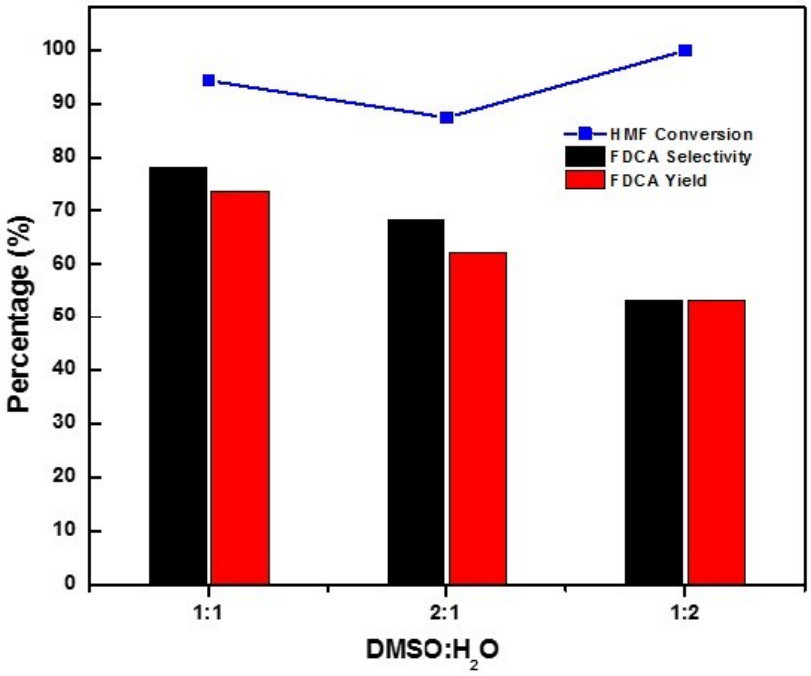

Figure S15. Effect of DMSO/H_2O content ratios for 8 h reaction at conditions (110 ^oC, 40 Bar O_2)

. As can be seen in Figure S15, 1:1 of DMSO and water concentration demonstrated the superior catalytic efficiency in terms of FDCA selectivity and yield as a result of faster mass transfer kinetics. After 8 hours of reaction time (T = 110 ^oC, P(O_2) = 40 bar, HMF: Fe = 30:1) in a solvent mixture with a DMSO:H_2O ratio of 1:1, the highest FDCA yield of 73.7% was achieved, which gradually decreased with further increase in DMSO (2:1) as well as water (1:2) content. These results are in agreement with Liu Huai et al. who reported that humins formation are generally suppressed in DMSO/H_2O mixture as compared to either pure DMSO or pure water.[9]

Table S3. Screening of highly efficient catalyst for HMF oxidation to FDCA

Entry	Catalysts	HMF Conversion (%)	FDCA Selectivity (%)	FDCA Yield (%)	HMFCA Yield (%)	FFCA Yield (%)	DFF Yield (%)
01	No catalyst	3.2	-	-	-	-	-
02	γ-Al_2O_3	11.8	23.1	2.72	-	-	-
03	Fe-N-C*	42.9	26.5	11.4	27.4	-	2.5
04	Fe-N-C/γ-Al_2O_3	99.9	99.9	99.8	-	0.1	-
05	Fe-N-C/TiO_2	97.4	71.4	69.6	0.5	-	14.3
06	Fe-N-C/ZrO_2	89.5	62.1	55.6	9.3	14.2	9.4
07	Fe-N-C/MgO	7.6	98.8	7.5	-	-	-

Reaction Conditions: 0.8 mmol HMF, 150 mg catalyst, HMF/Fe 30:1, 10 mL DMSO/H_2O, 110 ^oC, 40 bar O_2, 15 h **HPLC Conditions:** Rezex ROA Organic Acid Column H^+ (8%), 5 mM H_2SO_4, 0.5 mL/min, 45 ^oC, 1 h. *Support leached using 1 M HNO_3 solution.

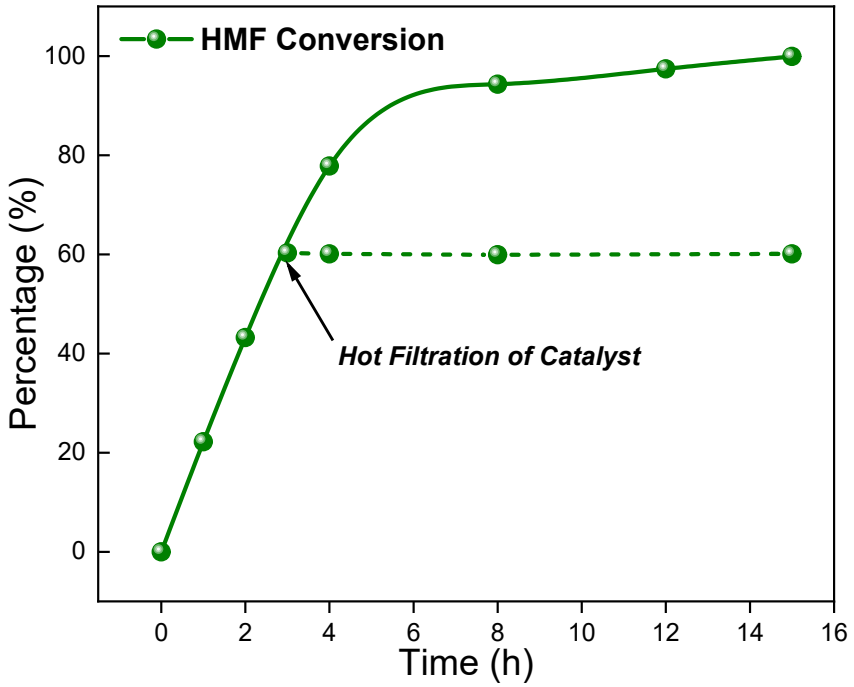

Figure S16. Hot-filtration test of Fe-N-C/γ-Al_2O_3 catalyst during oxidation of HMF.

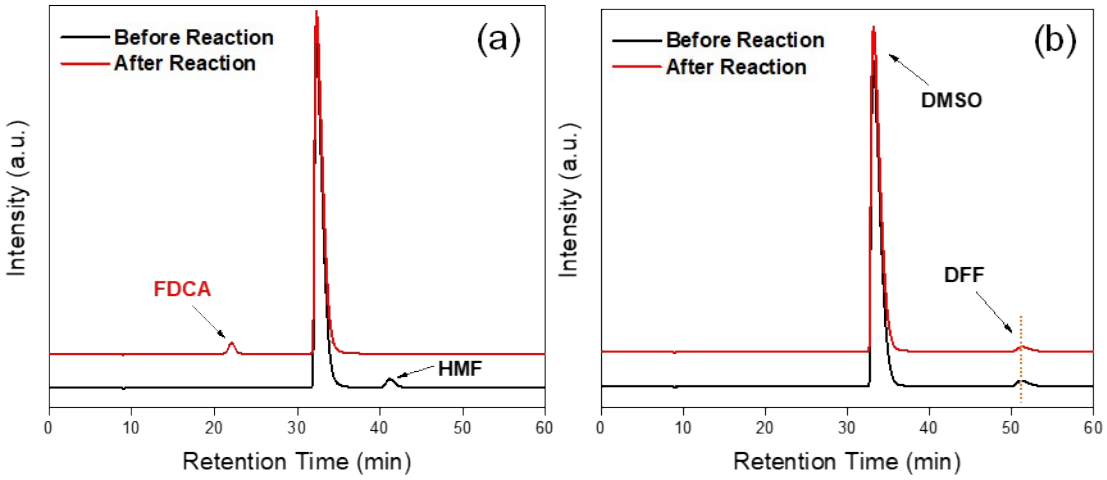

Figure S17. Comparison of HPLC chromatograms oxidation reaction using **(a)** HMF as substrate **(b)** DFF as substrate over Fe-N-C/γ-Al_2O_3 catalyst under optimized reaction conditions. **Reaction Conditions**: 0.8 mmol DFF, 150 mg catalyst, DFF/Fe 30:1, 10 mL DMSO/H_2O, 110 °C, 40 bar O_2, 15 h **HPLC Conditions:** Rezex ROA Organic Acid Column H^+ (8%), 5 mM H_2SO_4, 0.5 mL/min, 45 °C, 1 h. *The retention times for FDCA, HMFCA, HMF, and DFF were 21.9, 28.3, 29.7, 41.1 and 51.2 respectively.

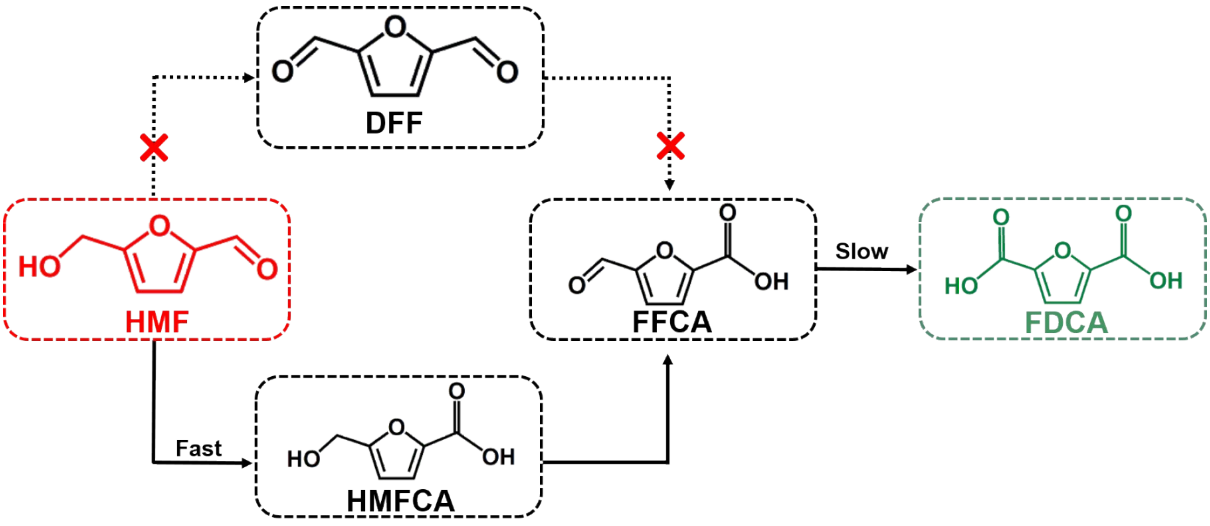

Scheme S1. Possible route of HMF oxidation to FDCA over Fe-N-C/γ-Al_2O_3 catalyst

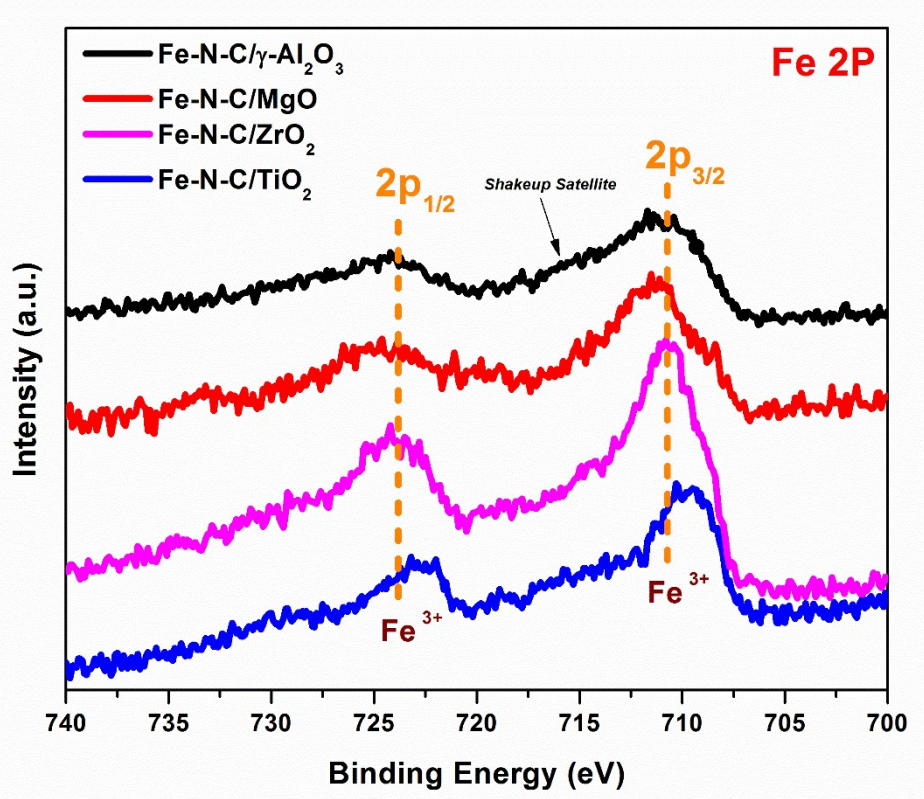

Figure S18. XPS (Fe 2p) spectra for supported Fe-N-C catalysts

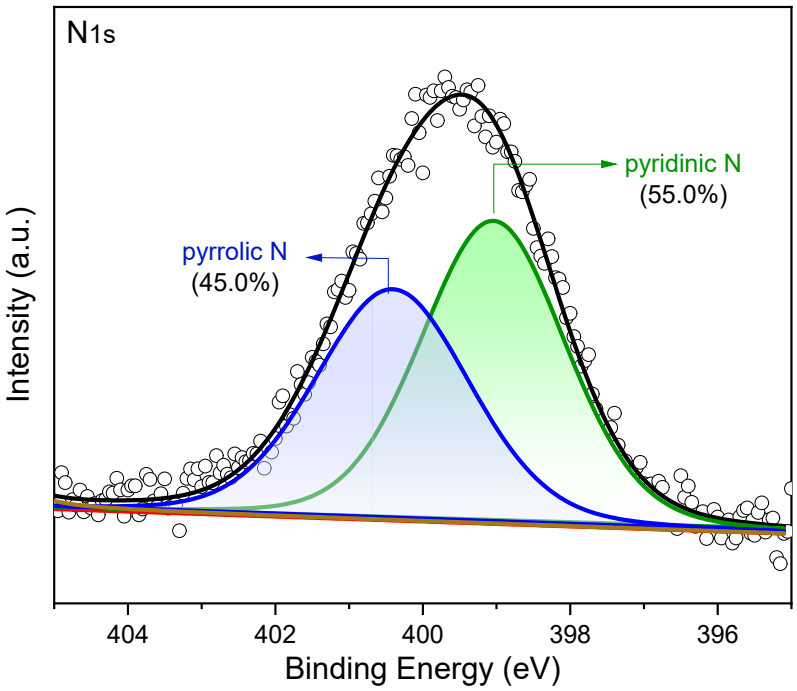

Figure S19. XPS (N 1s) spectra for Fe-N-C/γ-Al_2O_3 catalyst

Table S4. Curve fit Parameters for Fe K-edge EXAFS for sample [a]

Sample	Path	*R*(Å)	*N*	ΔE_0 (eV)	σ^2 (Å^2)	R factor (%)
Fe Foil	Fe-Fe_1	2.46+/-0.01	8[b]	5.3+/-1.0	0.005+/-0.001	0.6
	Fe-Fe_2	2.85+/-0.01	6[b]		0.005+/-0.001	
Fe-N-C/γ-Al_2O_3	Fe-N_1	1.96+/-0.02	3.4+/-0.7	0.8+/-1.7	0.003+/-0.001[c]	1.1
	Fe-N_2	2.07+/-0.03	2.0+/-0.3		0.003+/-0.001[c]	
Fe-N-C/γ-Al_2O_3-spent	Fe-N_1	2.00+/-0.02	3.3+/-0.8	-2.2+/-2.8	0.003+/-0.001[c]	3.0
	Fe-N_2	2.08+/-0.03	2.2+/-0.5		0.003+/-0.001[c]	

[a] S_0^2 was fixed as 0.73. Data ranges: $3.0 \leq k \leq 12.0$ Å^{-1}, $1.0 \leq R \leq 2.5$ Å ($1.0 \leq R \leq 2.5$ Å for Fe foil). The variable parameters number is 6, out of a total of 8.4 independent data points for "Fe-N-C/γ-Al_2O_3" and "Fe-N-C/γ-Al_2O_3-spent". [b] The coordination number for Fe-Fe was fixed as 8 and 6 based on Fe foil crystal structure (Fe mp-13). [c] The Debye-Waller factors were constrained as σ^2(Fe-N_1) = σ^2(Fe-N_2) for directly coordination between Fe and N in the same shell and reduce variable parameters number at the same time.

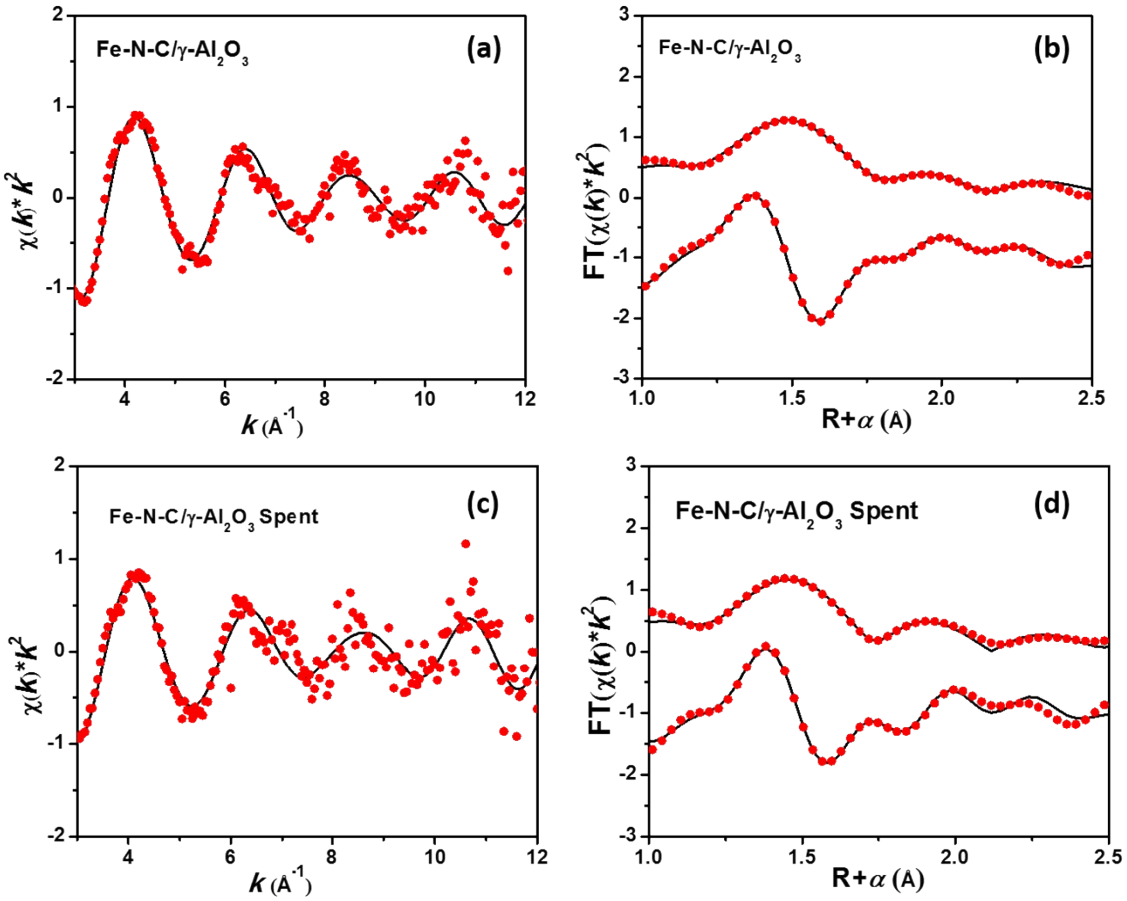

Figure S20. Fe K-edge EXAFS (points) and the curve fit (line) for fresh and spent Fe-N-C/γ-Al_2O_3 catalysts, shown in k-space and R-space (FT magnitude and imaginary component). The data is k^2-weighted and not phase-corrected.

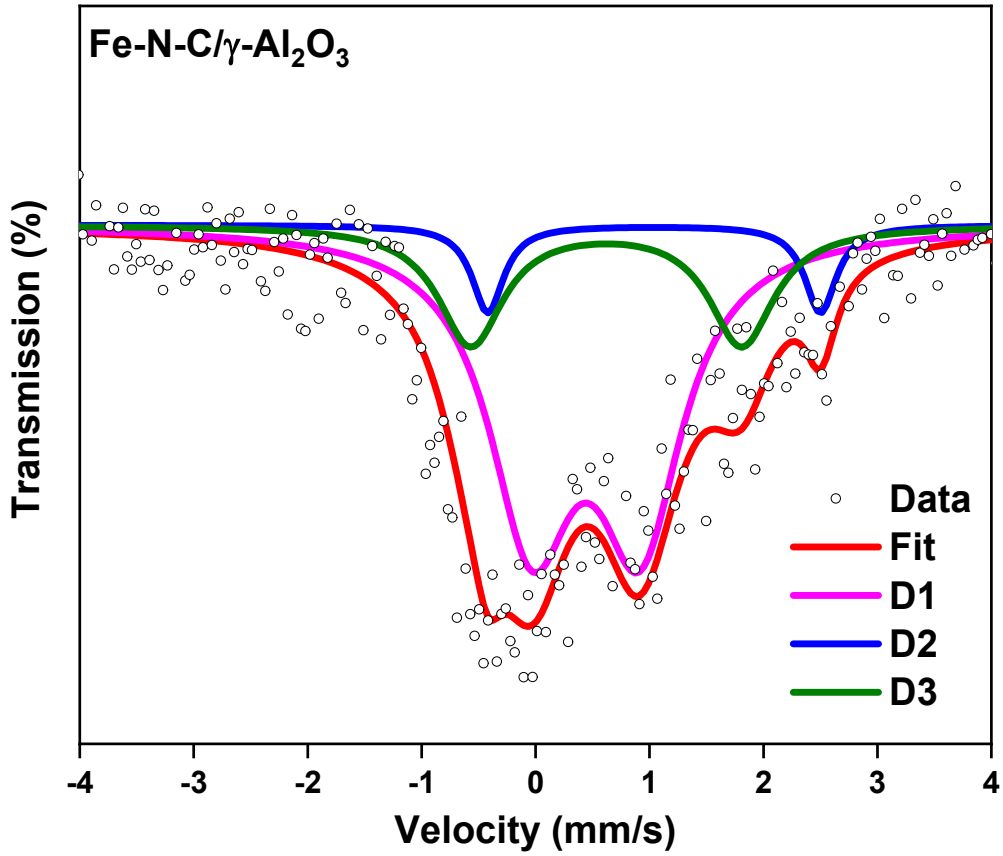

Figure S21. ^{57}Fe Mössbauer spectra of the Fe-N-C/γ-Al_2O_3 catalyst.

Table S5. Mössbauer parameters and relative absorption area obtained for each component from the fitting of the experimental spectrum recorded at room temperature. The isomer shift is given *versus* that of α-Fe.

Sites	δ (mm s^{-1})	ΔE_Q (mm s^{-1})	Γ (mm s^{-1})	A (%)	Assignment
Doublet (D1)	0.44	0.95	0.90	70.1	N-FeN_4-N, low-spin
Doublet (D2)	1.04	2.91	0.33	7.8	FeN_4-N, mid-spin
Doublet (D3)	0.62	2.37	0.69	22.0	X-FeN_4-Y (X/Y ligand like: O/N), high-spin

***δ** = Isomer Shift relative to α-iron, **ΔE_Q** = Quadrupole Splitting **Γ** = Line Width **A** = Relative area*

Table S6. Acidic-basic properties of the catalysts.

Entry	Catalyst	NH_3-TPD (Acidity)		CO_2-TPD (Basicity)	
		Temperature at maximum (°C)	Quantity (μmol g^{-1})	Temperature at maximum (°C)	Quantity (μmol g^{-1})
01	Fe-N-C/γ-Al_2O_3	119	381	514	269
02	Fe-N-C/MgO	109	55	596	341
03	Fe-N-C/ZrO_2	103	116	535	177
04	Fe-N-C/TiO_2	156	289	294	138

**All samples are calcinated at 700 °C for 2 h in N_2 atmosphere*

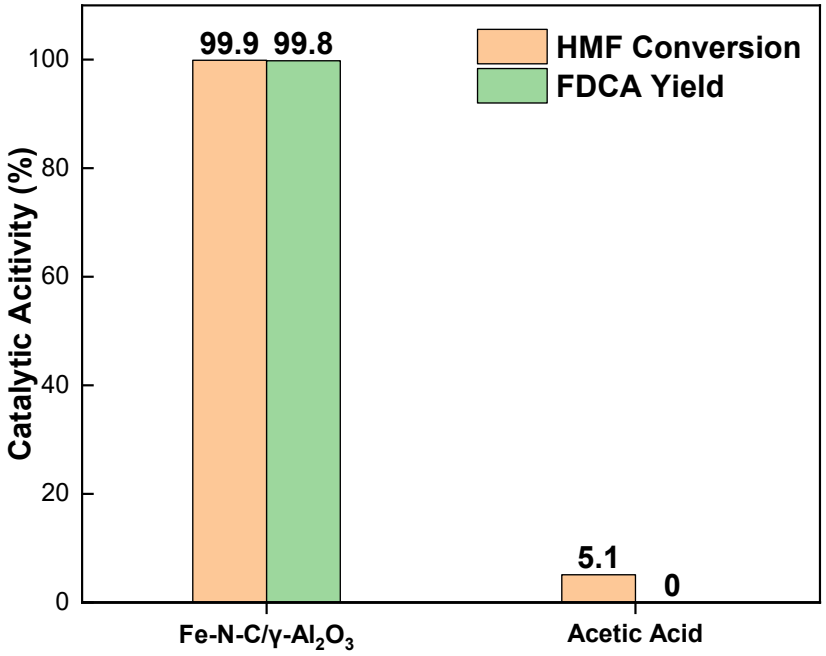

Figure S22. Comparison of HMF oxidation in the presence of catalyst and strong organic acid. Reaction Conditions: 0.8 mmol HMF, 150 mg catalyst, HMF/Fe 30:1, 10 mL DMSO/H_2O, 110

°C, 40 bar O_2, 15 h. HPLC Conditions: Rezex ROA Organic Acid Column H^+ (8%), 5 mM H_2SO_4, 0.5 mL/min, 45 °C, 1 h.

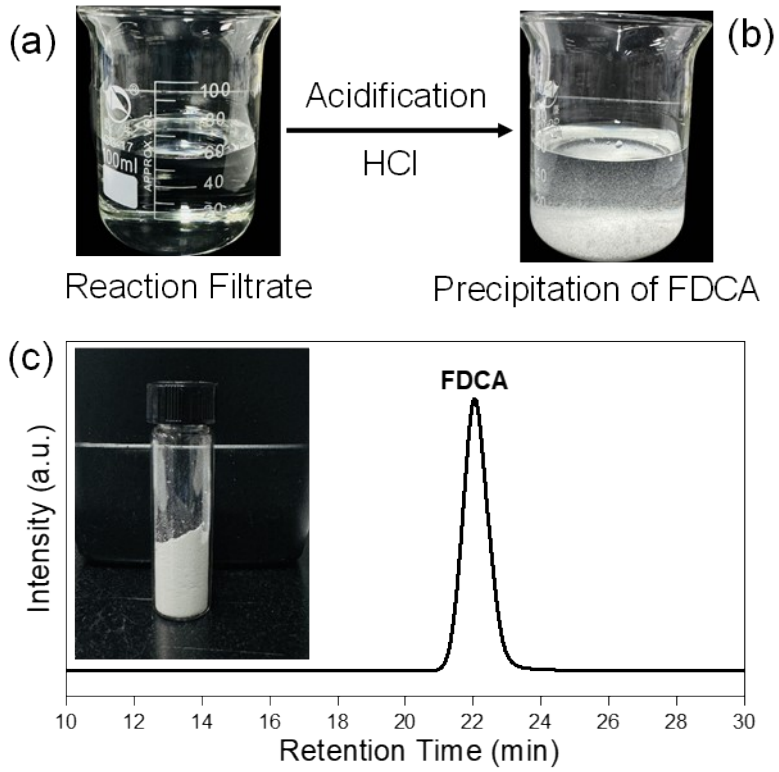

Figure S23. Gram Scale experiment and isolation of FDCA. (a) Reaction filtrate after recycling catalyst (b) Precipitation of FDCA after acidification with HCl (pH~1) (c) HPLC chromatogram of isolated FDCA (the inset picture is freeze dried FDCA, 0.63 g, 72.6% of isolated Yield). Reaction Conditions: 5.4 mmol HMF, 1 g Fe-N-C/γ-Al_2O_3 catalyst, HMF/Fe 30:1, 60 mL DMSO/H_2O, 110 °C, 40 bar O_2. HPLC Conditions: Rezex ROA Organic Acid Column H^+ (8%), 5 mM H_2SO_4, 0.5 mL/min, 45 °C, 1 h.

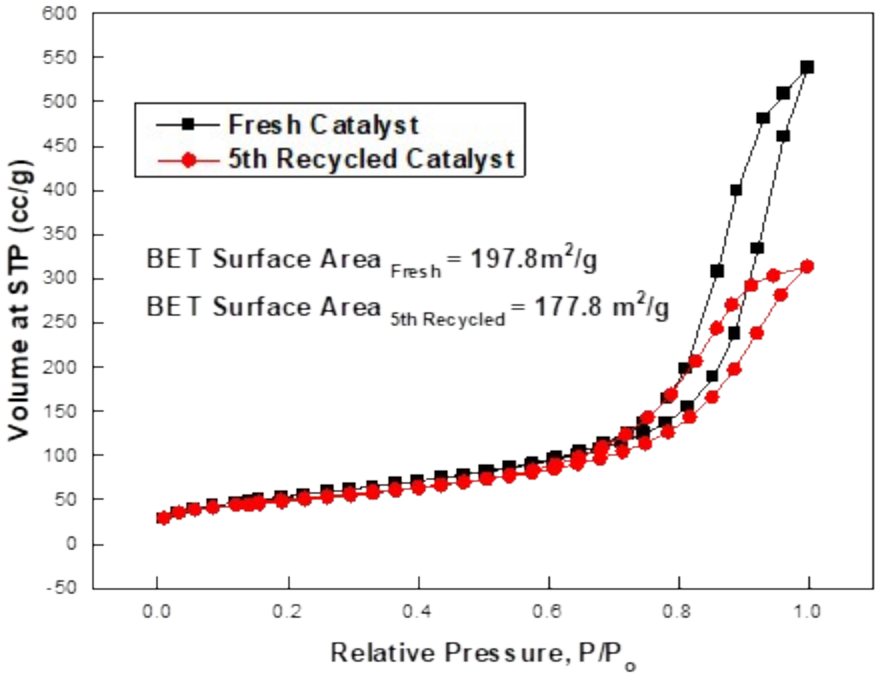

Figure S24. BET isotherms for fresh and fifth time recycled catalyst

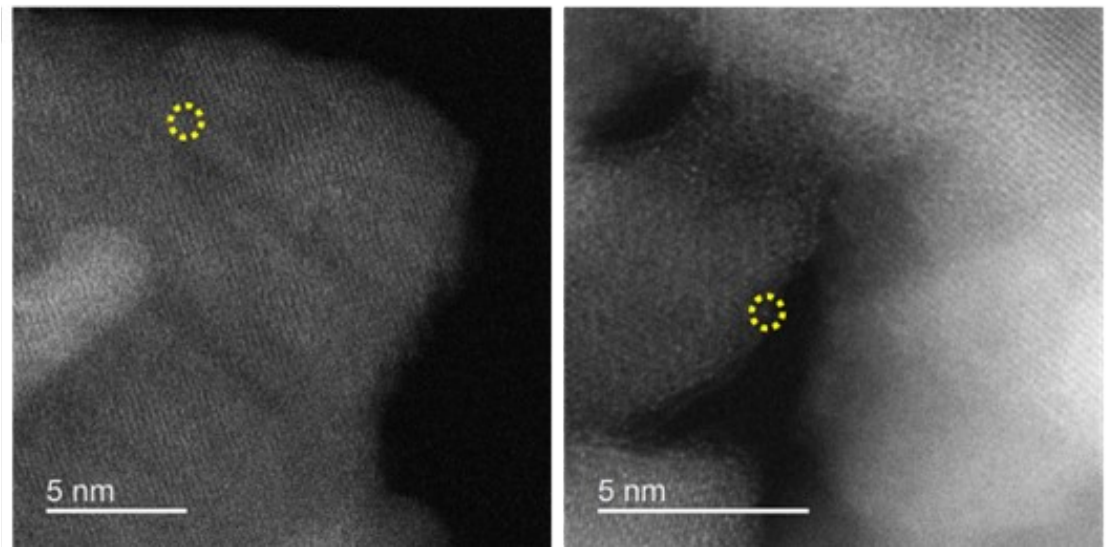

Figure S25 (c) HAADF-STEM images of the Fe-N-C/γ-Al_2O_3 catalyst after six catalytic runs.

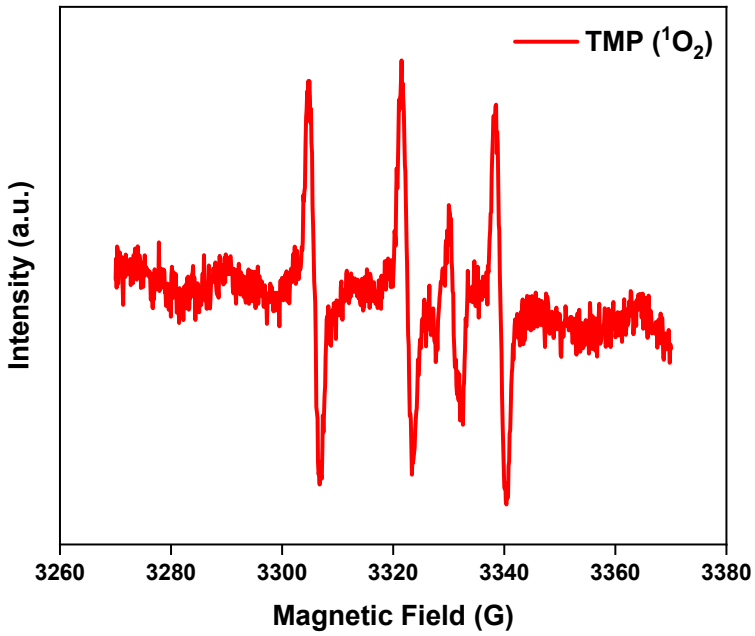

Figure S26. Spin trapping EPR signals of TMP-$^1O_2$ adduct in the presence of Fe-N-C/γ-Al_2O_3 catalyst. The spectrum was recorded after 30 min of introducing TMP in the reaction system.

References

1 D. Gao, F. Han, G. I. Waterhouse, Y. Li, L. Zhang, ACS Sustain. Chem. Eng., 2023.

2 S. A. A. Vandarkuzhali, G. Karthikeyan, M. Pachamuthu, Molecular Catalysis, 2021, **516,** 111951.

3 A. Tirsoaga, M. El Fergani, N. Nuns, P. Simon, P. Granger, V. I. Parvulescu, S. M. Coman, Appl. Catal., B: Environ., 2020, **278,** 119309.

4 D. Yan, J. Xin, Q. Zhao, K. Gao, X. Lu, G. Wang, S. Zhang, Catalysis Science & Technology, 2018, **8,** 164-175.

5 D. Yan, J. Xin, C. Shi, X. Lu, L. Ni, G. Wang, S. Zhang, Chemical Engineering Journal, 2017, **323,** 473-482.

6 S. Wang, Z. Zhang, B. Liu, ACS Sustainable Chemistry & Engineering, 2015, **3,** 406-412.

7 B. Saha, D. Gupta, M. M. Abu-Omar, A. Modak, A. Bhaumik, Journal of catalysis, 2013, **299,** 316-320.

8 W. Tang, X. Wu, D. Li, Z. Wang, G. Liu, H. Liu, Y. Chen, Journal of Materials Chemistry A, 2014, **2,** 2544-2554.

9 H. Liu, X. Cao, T. Wang, J. Wei, X. Tang, X. Zeng, Y. Sun, T. Lei, S. Liu, L. Lin, J. Ind. Eng. Chem., 2019, **77,** 209-214.